Direct observation of the electron-phonon coupling between empty states in graphite via high-resolution electron energy-loss spectroscopy

Shin-ichiro Tanaka*
The Institute of Scientific and Industrial Research, Osaka University, 8-1 Mihogaoka, Ibaraki, Osaka 567-0047, Japan

Kozo Mukai and Jun Yoshinobu
Institute for Solid State Physics, The University of Tokyo, Kashiwanoha 5-1-5, Kashiwa, Chiba 277-8581, Japan
(Received 19 January 2017; revised manuscript received 3 March 2017; published 7 April 2017)

Electron-phonon coupling (EPC) in graphite was investigated via high-resolution electron energy-loss spectroscopy and first-principles band calculations. We found strong resonance enhancements in the magnitude of specific phonon scatterings at specific primary energies of the incident electron. This result is attributed to a new scattering mechanism, where the incident electron is trapped at an unoccupied band, is scattered into another band via EPC with a specific phonon, and is finally detected by the analyzer. The scattering intensity is related to the electron-phonon matrix element wherein the energy and momenta of both electron and phonon are resolved.

DOI: 10.1103/PhysRevB.95.165408

I. INTRODUCTION

Electron-phonon coupling (EPC) is one of the most important topics in condensed matter physics [1–3]. EPC is usually examined in terms of the Eliashberg function [2,4,5], which is expressed as follows:

$$\alpha^2 F_{\mathbf{k},i}(\hbar\omega) = \sum_{\nu} \int_{\mathbf{q}} \delta(\omega - \omega_{\mathbf{q},\nu}) \delta(\epsilon_{\mathbf{k},i} - \epsilon_{\mathbf{k}\pm\mathbf{q},j} \pm \hbar\omega_{\mathbf{q},\nu}) \times \langle \phi_{\mathbf{k}\pm\mathbf{q},j} | \hat{H}_{\mathbf{q},\nu} | \phi_{\mathbf{k},i} \rangle d\mathbf{q},$$

where $\epsilon_{\mathbf{k},i}$ is the energy of the electron whose band index and momentum are i and $\mathbf{k}$, respectively. $\omega_{\mathbf{q},\nu}$ is the energy of the phonon whose branch index and momentum are ν and $\mathbf{q}$, respectively. The elemental quantity is the electron-phonon matrix element $\langle \phi_{\mathbf{k}\pm\mathbf{q},j} | \hat{H}_{\mathbf{q},\nu} | \phi_{\mathbf{k},i} \rangle$, which reflects the probability of electrons scattering from the initial state $\phi_{\mathbf{k},i}$ to the final state $\phi_{\mathbf{k}\pm\mathbf{q},j}$ via a phonon with $\mathbf{q}$ and ν. The electron momenta $\mathbf{k}+\mathbf{q}$ and $\mathbf{k}-\mathbf{q}$ correspond to the phonon absorption and emission processes, respectively. However, conventional methods, e.g., angle-resolved photoelectron spectroscopy (ARPES) and optical spectroscopy, have not resolved this matrix element from the Eliashberg function. Therefore, it is highly desirable to experimentally investigate the probability of electron-phonon scattering while resolving all quantities, i.e., i, j, ν, $\mathbf{k}$, and $\mathbf{q}$, in order to comprehensively understand EPC.

Previous studies have shown that the coupling between the vibration and electronic states of an adsorbed molecule can be investigated using high-resolution electron energy-loss spectroscopy (HREELS) on solid surfaces [6–8]. This phenomenon is known as the negative-ion resonance scattering mechanism wherein incoming electrons are temporarily trapped at the unoccupied molecular orbital to form a negative ion as shown in the left-hand side of Fig. 1. Subsequently, electrons are ejected, accompanied by the excitation of molecular vibrations due to electron-vibration coupling as shown in the right-hand side of Fig. 1. However, to the best of our knowledge, there has been no study investigating EPC in a single crystal while resolving the momentum of the phonon via HREELS. The resonance enhancement in the intensity of the phonon loss peaks depends on the kinetic energy of the incident electron beam (referred to as the primary energy hereafter), which is considered to be an experimental evidence for negative-ion resonance scattering, and has been observed in several surfaces [7,9–11]. However, no phonon dispersion or phonon selectivity has been reported.

In this paper, we demonstrate experimental evidence for observations of electron-phonon scattering between specific empty bands of graphite using HREELS. Highly ordered pyrolytic graphite (HOPG) is chosen as a target material because (i) it is a basic material for investigating carbon nanomaterials (e.g., graphene), where EPC is particularly important in achieving high-quality electronic devices, and (ii) it is easy to obtain a clean surface and it is very inert against contamination.

II. EXPERIMENTS

Experiments were performed in an ultrahigh vacuum chamber, with a base pressure of better than 1×10^{-10} Torr, equipped with an HREELS spectrometer (ELS5000, LK Technologies). An energy resolution of 2.5–3 meV (tested in the direct mode) was used. The incidence and detection angles were controlled by the rotations of both the sample and the electron analyzer around the axis perpendicular to the scattering plane. Throughout the research, the peak intensities are normalized to the elastic-peak area intensity within ± 1 meV in the loss (gain) energy because it is much more reliable than the absolute intensity, which is extremely sensitive to the electrostatic condition of the spectrometer's lenses. A commercially distributed HOPG sample (ZYB grade; IBS-MikroMasch) was cleaved in air, cleaned via heating at 800 °C for more than 60 min under a pressure of $<2 \times 10^{-8}$ Torr, and checked using HREELS. All measurements were performed at room temperature.

*stanaka@sanken.osaka-u.ac.jp

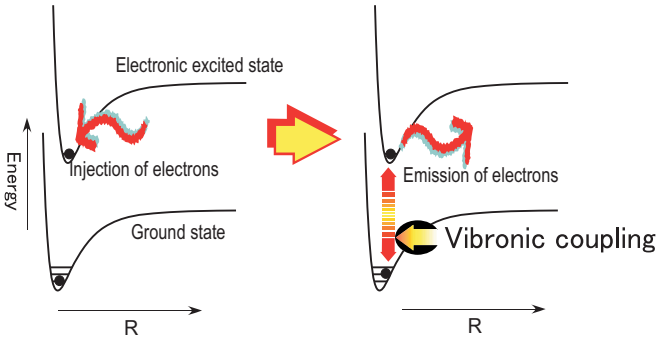

FIG. 1. Schematic diagram of the negative ion resonance scattering mechanism in the high-resolution electron energy-loss spectroscopy (HREELS) for the molecular adsorbates on the solid surface.

III. RESULTS

Figure 2 shows the HREELS spectra obtained at the primary energies (E_p) of [Fig. 2(a)] 19.0 eV, [Fig. 2(b)] 10.7 eV, and [Fig. 2(c)] 6.9 eV. The parallel momentum of the electron can be calculated as follows: $0.512\sqrt{E_k}\sin(\theta)$, where E_k and θ denote the kinetic energy and the angle from the surface normal, respectively, of the electron beam. The differences in the parallel momentum between the incident and detected electrons were all 0.34 Å^{-1} in Figs. 2(a)–2(c). In the case of the primary energy of 19 eV, several peaks were observed and attributed to phonon bands at a parallel momentum ($|\mathbf{q}_{//}|$) of 0.34 Å^{-1} compared to previous HREELS and theoretical studies [13–18]. The peaks from the lower loss energy are attributed to the ZA, ZO′, TA, LA, ZO, TO, and LO modes, where Z, T, and L indicate the out-of-plane, in-plane-transverse, and in-plane-longitudinal modes of graphite,

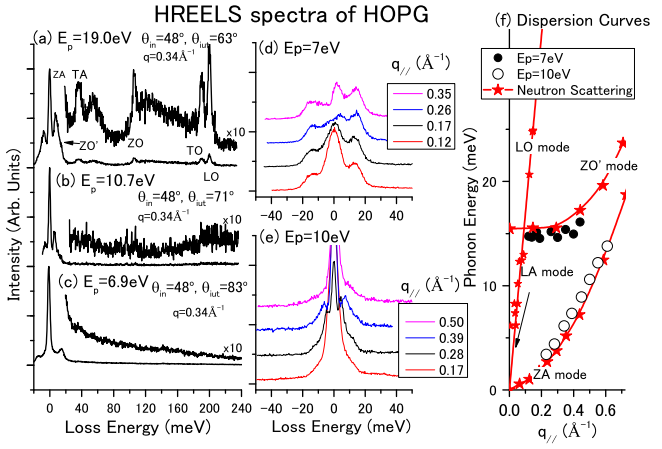

FIG. 2. (a)–(c) HREELS spectra of highly ordered pyrolytic graphite (HOPG) with different E_p's. The incident and detection angles of the electron beam are shown in the figure. The primary energies (E_p) are (a) 19.0 eV, (b) 10.7 eV, and (c) 6.9 eV. (d) and (e) Angle-dependent HREELS spectra obtained at $E_p = 7.0$ eV (d) and 10.0 eV (e). The parallel momenta of the phonon ($q_{//}$) are indicated. (f) Comparison of the phonon dispersion curves derived from the presented experiments (● and ○) and neutron scattering (★) [12].

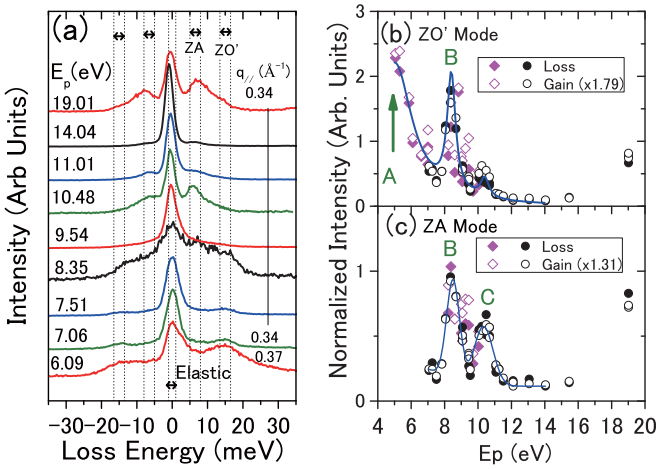

FIG. 3. (a) Series of HREELS spectra for HOPG as a function of the E_p's. (b) and (c) Gain/loss intensities of the ZO′ (b) and ZA (c) modes. The lines provide a guide for the eye.

respectively, and A and O indicate the acoustic and optical modes, respectively.

When the primary energy decreases to 10.7 eV [Fig. 2(b)] or 6.9 eV [Fig. 2(c)], the HREELS spectra drastically changes. The peaks whose energies were higher than 20 meV are nearly extinguished, and only the (b) ZA or (c) ZO′ modes are observed. To study this in more detail, we measured the dispersion of the phonons obtained at 7.0 eV [Fig. 2(d)] and 10.0 eV [Fig. 2(e)]. Here, the angle between the monochromator and the analyzer was fixed to 120° and the sample was rotated. The corresponding $|\mathbf{q}_{//}|$ value is indicated in the figure. The peak positions were determined by deriving a secondary differentiation of the HREELS spectra [spectra in addition to those shown in Figs. 2(d) and 2(e) were also obtained] and are plotted in Fig. 2(f) as a function of $|\mathbf{q}_{//}|$, which agrees well with the dispersion curves of the ZO′ ($E_p = 7$ eV) and ZA ($E_p = 10$ eV) modes derived via the neutron-scattering method [12]. Although both are interlayer (out-of-plane) vibrational modes dispersing along the surface normal ($\mathbf{q}_z$), the phonon energies observed here still agree with dispersion along the Γ-K and Γ-M lines at $\mathbf{q}_z = 0$.

To comprehensively investigate the resonance behavior, the E_p dependence of the HREELS spectra was measured. In Fig. 3(a), series of HREELS spectra are shown along with E_p. In the spectra from $E_p = 7.06$ eV to $E_p = 19.01$ eV, the incident angle of the electron beam was fixed to 48° and the detection angle was changed from 82° to 63° while $|\mathbf{q}_{//}|$ was maintained at 0.34 Å^{-1}; in the spectra with E_p less than 7 eV, the incident and detection angles were fixed to 43° and 77°, respectively, where the corresponding $|\mathbf{q}_{//}|$'s are indicated in the figure. The loss and gain peaks ascribed to ZA and ZO′ are observed from 5(−8) meV to 8(−5) meV and from 13.5(−16.5) to 16.5(−13.5) meV, respectively, which are indicated by dotted lines in Fig. 3(a). Obviously, the intensities of these peaks are strongly dependent on E_p. In Figs. 3(b) and 3(c), the area intensities for the ZA and ZO′ photon scatterings, respectively, within the indicated energy region are plotted as a function of E_p. The solid and open diamonds (♦ for gain and ◇ for loss) were derived from the

spectra obtained at the fixed incident and detection angles (43° and 77°, respectively), where $|\mathbf{q}_{//}|$ changes from 0.34 Å^{-1} (5.1 eV) to 0.47 Å^{-1} (10.0 eV) and the solid and open circles (● for loss and ○ for gain) were derived from the spectra, where the incident angle was fixed to be 43° and the detection angle was changed in order to produce a fixed $|q_{//}|$ of 0.34 Å^{-1} [the detection angle was changed from 82° (7.1 eV) to 63° (19.0 eV)]. In Figs. 3(b) [3(c)], the intensities of gain peaks are multiplied by 1.79 (1.31), which was derived from $\exp(\frac{\hbar\omega}{k_B T})$, where $\hbar\omega$ is the phonon energy, k_B is the Boltzmann constant, and T is the temperature (300 K) [19]. The overall agreements in the intensities between the energy loss and the energy gain after this multiplication are reasonable over the entire E_p range, suggesting that the measurements were performed with considerable accuracy. In Fig. 3(c), the intensity of the ZA phonon is not plotted below an E_p of 7 eV because it is obviously obscured by the ZO′ phonon, as shown in Fig. 3(a). Although the intensities are somewhat scattered, the structures are clearly seen. The solid lines in Figs. 3(b) and 3(c) are drawn to aid the eye and are made by two distinct peaks (the Lorentzian peak shape is assumed here) at 8.4 eV (B) and 10.4 eV (C) and a large increase below 7 eV for the ZO′ intensity. For convenience, we will refer to the structure below 7 eV as peak A at 5 eV even though it may not be a peak or located below 5 eV.

IV. DISCUSSION

There are three different scattering interactions that can be probed using HREELS: dipole, impact, and negative-ion resonance scattering [6–8]. However, the above-mentioned behavior of the HREELS spectra at $E_p < 14$ eV cannot be explained by any of these interactions. Dipole scattering, wherein an electric field accompanied by a moving electron interacts with the dipole field created by atomic vibration, dominates only in specular reflection. Impact scattering, which occurs due to short-range interactions between electrons and moving nuclei of atoms, is thought to be responsible for phonon probing in HREELS. In fact, the HREELS spectrum obtained at $E_p = 19$ eV [Fig. 2(a)] is thought to be the result of impact scattering, similar to that in previous studies [13–16]. However, impact scattering is not favored by low E_p, and the strong resonance behavior at $E_p < 12$ eV can hardly be explained by the impact scattering mechanism. As will be discussed later, the oscillation of the elastic peak intensities as a function of E_p may cause the oscillation of the relative loss/gain peak intensities. However, this should similarly affect all the phonon modes if the impact scattering mechanism works, and therefore, the selection of the phonon modes with E_p, as observed in peaks A and C, cannot be explained.

As noted earlier, the negative-ion resonance mechanism is a model for molecular vibrations adsorbed on the surface and is not suitable for phonon scattering in graphite. Nevertheless, the characteristics observed here, i.e., a resonance behavior depending on E_p and the selection of the phonon modes, are very similar to those observed in the negative-ion resonance scattering mechanism [6–8]. Therefore, it seems straightforward to attribute it to a similar mechanism, i.e., a coupling between the unoccupied wave functions and the

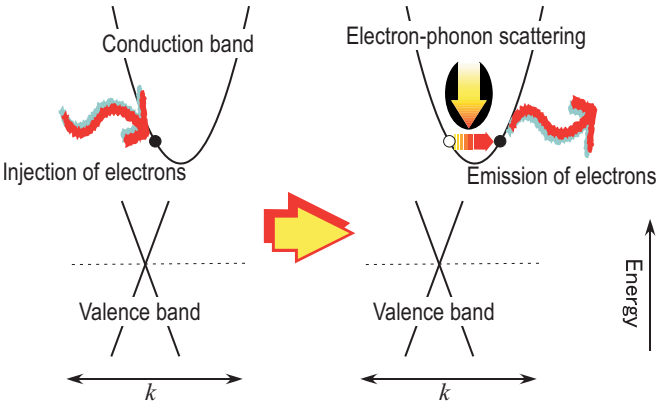

FIG. 4. Schematic diagram of the newly proposed scattering mechanism depicted in the inverse-lattice space.

atomic motion, which are not the motions of the molecular orbital and vibration but the electronic band and phonon in graphite with a translational symmetry. In this newly proposed scattering mechanism whose diagram is shown in Fig. 4, the injected electron is temporarily trapped at a certain point in the unoccupied electron band [20], scattered into another band as a result of EPC, and ultimately detected by the electron detector. Note that the first and last processes, where the plane wave of the incoming and outgoing electron beams are connected with the wave functions in the solid-solid surface, resembles the photoelectron emission process in the one-step model of photoelectron spectroscopy [21]. The striking difference of this from negative-ion resonance is that it requires the conservation of not only the energy but also the parallel momentum. An additional striking difference from impact scattering is that the wave function interacting with the phonon is the unoccupied band of graphite instead of the plane wave in impact scattering. Therefore, the resonance enhancement in the scattering intensity requires the following conditions: (i) the energy and parallel momentum of the incident-end ejected electron beams must match those of the unoccupied bands and (ii) the matrix element $\langle\phi_{\mathbf{k}\pm\mathbf{q},j}|\hat{H}_{\mathbf{q},\nu}|\phi_{\mathbf{k},i}\rangle$ must have a considerable magnitude.

To confirm the former conditions, we compared the resonance condition observed in the HREELS measurement with the unoccupied band structure of HOPG. In previous studies of HOPG, the experimental results were often compared to those of the band dispersion along the high-symmetry lines (the Γ-K-M and Γ-M lines) [22]. However, in HOPG, the azimuth of each graphene layer is randomly oriented, and therefore, in principle, such a comparison is questionable. Accordingly, we calculated the electronic structure of HOPG based on first-principles calculations [23,24] for the electronic structure of graphite in a similar way to that in our previous paper [25]. Figure 5 shows the calculated unoccupied electronic structure of HOPG, where the density of states is averaged around the Γ-A line and along the k_z axis as a function of $\mathbf{k}_{//}$ and as a color map from blue to red. Details of the calculation are described in the Supplemental Material [26], The electron energy is shown with respect to the Fermi level on the left-hand side. The cyan (green) lines in Fig. 5 show the relations of the electron energies of the incident (right lines) and detected

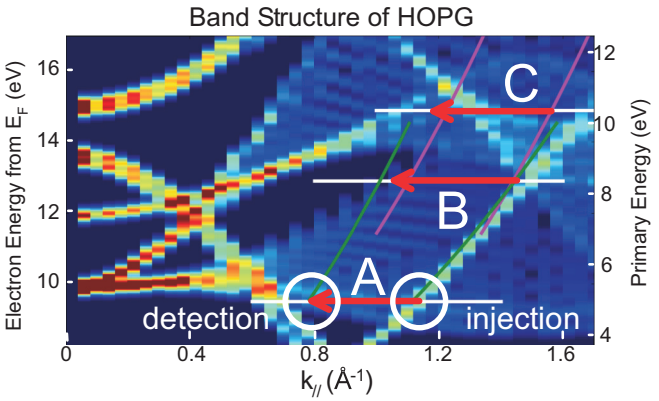

FIG. 5. Schematic of electron-phonon scattering between the unoccupied bands of graphite. The arrows on the A, B, and C lines show the scattering corresponding to the resonance condition indicated in Figs. 3(b) and 3(c). The unoccupied density of states for HOPG is presented as a color map. See the text and the second section of the supplemental materials for details.

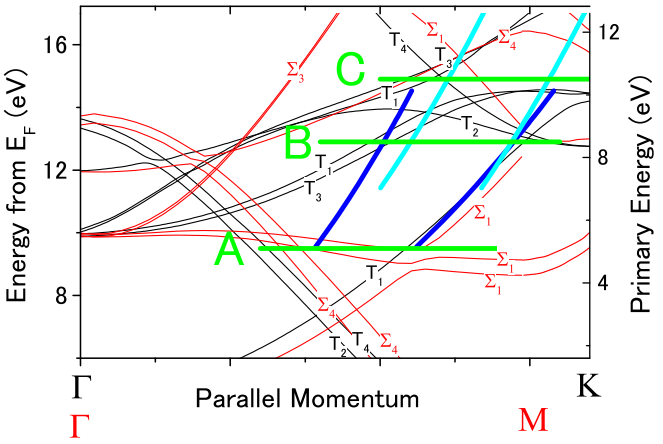

FIG. 6. Calculated band dispersions of graphite along the Γ-K (black, T-symmetry) and Γ-M (red, Σ-symmetry) lines. The symmetric character of the bands is indicated in the figure. The resonant condition in the high-resolution electron energy loss spectroscopy (HREELS) spectra is also shown as arrows A–C, similar to that shown in Fig. 5.

(left lines) electrons with respect to their parallel momenta in the measurements corresponding to the diamonds (circles) in Figs. 3(b) and 3(c), respectively. The white lines of A, B, and C indicate the kinetic energies, where the maximum in the relative intensities of the energy loss/gain peaks are observed in the HREELS spectra [Figs. 3(b) and 3(c)]. The energy scale is referenced to the vacuum level and indicated on the right-hand side, where the work function is assumed to be 4.5 eV. Therefore, the red arrows describe the electron-phonon scattering between the unoccupied bands and the base (head) of the arrow indicates the initial/injection (final/detection) point of the scattering, as described for transition A in Fig. 5. The loss/gain energies due to the phonon emission/absorption are neglected in the arrow because they are even smaller than the kinetic energy of the electrons.

This comparison shows that the resonances A and C approximately satisfy the the first condition and that the start and end points of the red arrows contain a considerable amount of the density of states of the unoccupied electron states. Small discrepancies could be observed due to the inaccuracy of the LDA calculation at the unoccupied electronic states. Moreover, the true position of resonance A may be lower than 5 eV, as noted earlier. However, it is difficult to conclude that there is an intense density of states near the end point of resonance B. According to a previous electron energy electron diffraction study [27], the (00) beam intensity is strongly enhanced at an electron energy of 8.6 eV, which is close to the kinetic energy of peak B (8.4 eV). This suggests that the off-specular elastic beam intensity is reduced at this kinetic energy, which may cause an enhancement of the relative loss/gain intensity. Therefore, peak B in Figs. 3(b) and 3(c) is not due to electron-phonon scattering but to the decrease in the elastic peak intensity. This interpretation is consistent with the fact that both the ZA and ZO′ modes are similarly enhanced at peak B. It should be also noted that the diffraction effect should affect the variation in the intensities in the HREELS spectra at any Ep's, and thus the position and shape of peaks A and B may not agree precisely with the electron density of states.

The agreement between the unoccupied band structure and the resonance condition suggests that the proposed scattering mechanism is reasonable. Therefore, the scattering intensity should also be governed by the intensity of the matrix element $\langle \phi_{\mathbf{k}\pm\mathbf{q},j} | \hat{H}_{\mathbf{q},\nu} | \phi_{\mathbf{k},i} \rangle$. In this case, when E_p in the HREELS was changed, the relevant band indexes changed. Subsequently, the phonon index necessary for producing a strong intensity of the electron-phonon matrix element changed. This leads to the selection of a phonon mode depending on E_p, and the reason why an E_p of 7 eV favors the ZO′ mode and an E_p of 10 eV favors the ZA mode can be attributed to the change in the intensity of the matrix element. The other phonon modes (all in-plane modes) were not observed, which may indicate a stronger coupling of the band electron with the interlayer vibration than the intralayer vibration of graphite.

The simplest and most important analysis of the selection rule should come from the symmetry of the relevant wave functions and the phonon, where scattering is allowed when the product of the characters for the initial and final wave functions and the phonon is totally symmetric. This is briefly discussed. First, it is assumed that scattering occurs on the high-symmetric lines (Γ-M and Γ-K) for simplicity. The space group of graphite is No. 194 in international tables of cystography, and the symmetry of the points where scattering occurs is Σ on the Γ-M line or T on the Γ-K line [28–30]. In Fig. 6, unoccupied band dispersions of graphite are shown along the Γ-K and Γ-M lines. The calculations were performed using OSAKA-2K codes, and the binding energy was expanded by 18%, as described in the previous section. The symmetry of the Hamiltonian operator of electron-phonon scattering is the same as that of the phonon [31]. To satisfy the condition that the total products of the bands and the phonon are totally symmetric (in this case, T_1 or Σ_1), transitions are allowed between the T_1 and T_4 (Σ_1 and Σ_4) bands [denoted as T_1/T_4 (Σ_1/Σ_4), hereafter] or T_2/T_3 (Σ_1/Σ_4) for the ZA mode of

TABLE I. The symmetry of the phonons along the Γ-K (symmetry: T) and Γ-M (symmetry: Σ) lines [28–30]; the allowed pairs of symmetry of the wave functions among which electron-phonon scattering occurs; and the possible resonant conditions derived from the symmetry of the unoccupied bands shown in Fig. 6.

Phonon	Symmetry	Allowed pair of wave functions	Possible transitions
LO	$T_3(\Sigma_1)$	$T_1/T_3, T_2/T_4$ (Σ_1/Σ_1, Σ_2/Σ_2, Σ_3/Σ_3, Σ_4/Σ_4)	B, C
TO	T_1 (Σ_3)	T_1/T_1, T_2/T_2, T_3/T_3, T_4/T_4 (Σ_1/Σ_3, Σ_2/Σ_4)	B, C
ZO	T_2 (Σ_4)	T_1/T_2, T_3/T_2 (Σ_1/Σ_4, Σ_2/Σ_3)	A, B, C
LA	T_1 (Σ_1)	T_1/T_1, T_2/T_2, T_3/T_3, T_4/T_4 (Σ_1/Σ_1, Σ_2/Σ_2, Σ_3/Σ_3, Σ_4/Σ_4)	B, C
TA	T_3 (Σ_3)	T_1/T_3, T_2/T_4 (Σ_1/Σ_3, Σ_2/Σ_4)	B, C
ZA	T_4 (Σ_4)	T_1/T_4, T_2/T_3 (Σ_1/Σ_4, Σ_2/Σ_3)	A, B, C
ZO′	T_4 (Σ_2)	T_1/T_4, T_2/T_3 (Σ_1/Σ_2, Σ_3/Σ_3)	A, B, C

the T_4 (Σ_4) symmetry and T_1/T_4 (Σ_1/Σ_4) or T_2/T_3 (Σ_3/Σ_4) for the ZO′ mode of the T_4 (Σ_2) symmetry, according to a simple calculation based on the character tables (Tables C.31 and C.32 of Ref. [28]). As shown in Fig. 6, possible transitions are Σ_1/Σ_4, T_1/T_2, and T_1/T_4 at line A; T_1/T_1, T_1/T_3, T_2/T_1, T_2/T_3, T_4/T_1, and T_4/T_1 at line B; and T_1/T_1, T_1/T_3, T_1/T_4, T_3/T_1, T_3/T_3, and T_3/T_4 at line C. Therefore, both the ZA and ZO′ phonons are allowed at any conditions of A–C from the viewpoint of symmetry. This means that the selection rule with symmetry does not explain why specific phonon modes are observed for specific transition conditions. The allowed pair of wave functions among which the electron-phonon transition occurs and the possible transitions at the resonant condition indicated by the A–C lines are listed in Table I. This reveals that other phonon modes besides ZA and ZO′ are also possible from the viewpoint of symmetry.

Therefore, the symmetry selection rule does not function properly in this case, and a more detailed analysis calculating the electron-phonon matrix element while resolving the momenta of the electron and the phonon [32] will be required to obtain a better understanding of the results observed in this research. Note that the scattering intensity depends not only on E_p (i.e., the band index) but also on the incident and detection angles (i.e., the momenta of the electron and the phonon). This is demonstrated in Fig. 2(c), where the intensity due to ZA phonon scattering obviously changes as a function of the value of $|\mathbf{q}_{//}|$, even though a quantitative analysis was difficult because the peak position is too close to the elastic peak. The scattering condition to be examined in this study is limited and additional studies will be necessary to fully understand EPC in graphite.

Recently, investigations concerning indirect transitions accompanying electron-phonon scattering in graphite conducted [32,33]. In these studies, electrons near the Fermi level located at the K point in the Brillouin zone were simultaneously excited by phonons and photons and directly detected using ARPES. The photon-energy dependence shows that electron-phonon scattering occurs between the unoccupied states located 6 eV (or below) from the Fermi level with ZA and/or ZO phonons and at 11.05 eV with TO and/or LO phonons. The condition 6.55 eV from the vacuum level is somewhat similar to condition A (5.0 eV from the vacuum level) at HREELS. However, the observed phonon modes, which scatter the electrons, are completely different (TO/LO in ARPES and ZO′ in HREELS). This is likely due to the scattering geometries in the Brillouin zone, i.e., the momenta of the electron and phonon, being considerably different in ARPES and HREELS. This is caused by the different freedoms of the positions of the samples and the analyzers during the measurements. Therefore, ARPES and HREELS are complementary techniques in terms of probing the electron-phonon scattering process. Moreover, in recent HREELS studies [34], Qin *et al.* evaluated the electron-phonon matrix element in cuprate $Bi_2Sr_2CaCu_2O_{8+\delta}$ using HREELS in a completely different approach than that used in this study. They estimated the matrix element from the peak width as a function of the phonon momentum q. Even though our method seems more straightforward, the wave functions they are dealing with are close to the Fermi edge, which has a more important effect on the properties of the matter than the unoccupied bands above several eV's in our study. Therefore, their method is thought to be complementary to ours.

V. CONCLUSION

In conclusion, HREELS was applied to investigate electron-phonon scattering in graphite. Contrary to the case with high primary energy (∼19 eV), where loss peaks due to all the phonon modes are observed as a result of the impact-scattering mechanism, only a few phonons (ZA and ZO′) are observed at lower primary energies ($E_p < 14$ eV). These loss (gain) intensities in the HREELS spectra exhibit strong resonance behaviors depending on the kinetic energy of the injected electron beam. These observations can be interpreted as the electron transition between the unoccupied bands via electron-phonon scattering, which is consistent with calculations of the unoccupied band structure of HOPG. Measuring the scattering intensities as functions of the primary energy and the angles of the electron beam, the intensity of the matrix elements of EPC can be evaluated between specific unoccupied bands via a specific phonon while resolving the momenta and energies of the electrons and phonons. Moreover, the band mapping of the unoccupied band is possible. Therefore, a combination of a multichannel electron spectrometer, which is commonly used for ARPES, and a high-resolution electron monochromator [35,36] would be more useful than conventional HREELS equipment because it not only significantly saves measurement time but also provides a wide range of the incident and detected angles of the electron beam.

This method is not limited to graphite and will be applicable to other materials in which EPC plays a crucial role in determining its properties, e.g., the BCS superconductor. The

application of this method will provide a good experimental basis for a deeper understanding of EPC in condensed matter.

ACKNOWLEDGMENTS

This research was conducted by the joint research in Institute for Solid State Physics, The University of Tokyo. It was supported by JSPS KAKENHI Grant No. T254003260 in Grant-in-Aid for Scientific Research (C) and JP25107003 in Scientific Research on Innovative Areas "Science of Atomic Layers". In addition, it was supported in part by Dynamic Alliance for Open Innovation Bridging Human, Environment and Materials from the Ministry of Education, Culture, Sports, Science and Technology of Japan (MEXT). The authors thank Professor K. Shirai from the Institute of Scientific and Industrial Research, Osaka University for distribution and support of his package OSAKA-2K.

[1] H. Haken, *Quantum Field Theory of Solids: An Introduction* (North-Holland, Amsterdam, 1976).
[2] G. Grimvall, *The electron-phonon interaction in metals*, Selected topics in solid state physics (North-Holland, Amsterdam, 1981).
[3] Y. Toyozawa, *Optical Processes in Solids*, Optical Processes in Solids (Cambridge University Press, Cambridge, 2003).
[4] J. Shi, S.-J. Tang, B. Wu, P. T. Sprunger, W. L. Yang, V. Brouet, X. J. Zhou, Z. Hussain, Z.-X. Shen, Z. Zhang, and E. W. Plummer, Phys. Rev. Lett. **92**, 186401 (2004).
[5] A. V. Fedorov, N. I. Verbitskiy, D. Haberer, C. Struzzi, L. Petaccia, D. Usachov, O. Y. Vilkov, D. V. Vyalikh, J. Fink, M. Knupfer, B. Büchner, and A. Grüneis, Nature Commun. **5**, 3257 (2014).
[6] H. Ibach and D. Mills, *Electron Energy Loss Spectroscopy and Surface Vibrations* (Academic Press, New York, 1982).
[7] P. Thirty, M. Liehr, J. Pireaux, and R. Caudano, Phys. Scr. **35**, 368 (1987).
[8] R. E. Palmer and P. J. Rous, Rev. Mod. Phys. **64**, 383 (1992).
[9] H. Conrad, M. Kordesch, and W. Stenzels, Surf. Sci. **178**, 578 (1986).
[10] K. W. Wulser and M. A. Langell, Phys. Rev. B **48**, 9006 (1993).
[11] J. Eggeling, G. R. Bell, and T. S. Jones, J. Phys. Chem. B **103**, 9683 (1999).
[12] R. Nicklow, N. Wakabayashi, and H. G. Smith, Phys. Rev. B **5**, 4951 (1972).
[13] J. Wilkes, R. Palmer, and R. Willis, J. Electr. Spec. Rel. Phenom. **44**, 355 (1987).
[14] C. Ohshima, T. Aizawa, R. Souda, Y. Ishizawa, and Y. Sumiyoshi, Solid State Commun. **65**, 1601 (1988).
[15] S. Siebentritt, R. Puse, K. H. Rieder, and A. M. Shikin, Phys. Rev. B **55**, 7927 (1997).
[16] H. Yanagisawa, T. Yorisaki, R. Niikura, S. Kato, Y. Ishida, K. Kamide, and C. Oshima, Phys. Rev. B **81**, 235430 (2010).
[17] L. Wirtz and A. Rubio, Solid State Commun. **131**, 141 (2004).
[18] M. Lazzeri, C. Attaccalite, L. Wirtz, and F. Mauri, Phys. Rev. B **78**, 081406R (2008).
[19] See Supplemental Material of Sec. I at http://link.aps.org/supplemental/10.1103/PhysRevB.95.165408 for the temperature dependence of the loss/gain ratio.
[20] E. G. McRae, Rev. Mod. Phys. **51**, 541 (1979).
[21] S. Hüfner, *Photoelectron Spectroscopy: Principles and Applications* (Springer, Berlin, 2003).
[22] S. Y. Zhou, G.-H. Gweon, C. D. Spataru, J. Graf, D.-H. Lee, S. G. Louie, and A. Lanzara, Phys. Rev. B **71**, 161403 (2005).
[23] K. Shirai, The source code is available at http://www.cmp.sanken.osaka-u.ac.jp/∼koun/osaka.html.
[24] K. Shirai and K. Yamanaka, J. Appl. Phys. **113**, 053705 (2013).
[25] S. Tanaka, Y. Takano, M. Okusawa, and K. Mase, J. Phys. Soc. Jpn. **83**, 084705 (2014).
[26] See Supplemental Material of Sec. II at http://link.aps.org/supplemental/10.1103/PhysRevB.95.165408 for the electronic structure of HOPG.
[27] J. J. Lander and J. Morrison, J. Appl. Phys. **35**, 3593 (1964).
[28] M. S. Dresselhaus, G. Dresselhaus, and A. Jorio, *Group Theory: Application to the Physics of Condensed Matter* (Springer, Berlin, 2008).
[29] M. S. Dresselhaus, G. Dresselhaus, P. C. Eklund, and D. D. L. Chung, Mater. Sci. Eng. **31**, 141 (1997).
[30] M. Mohr, J. Maultzsch, E. Dobardžić, S. Reich, I. Milošević, M. Damnjanović, A. Bosak, M. Krisch, and C. Thomsen, Phys. Rev. B **76**, 035439 (2007).
[31] M. Lax and J. J. Hopfield, Phys. Rev. **124**, 115 (1961).
[32] P. Ayria, S.-i Tanaka, A. R. T. Nugraha, M. S. Dresselhaus, and R. Saito, Phys. Rev. B **94**, 075429 (2016).
[33] S. Tanaka, M. Matsunami, and S. Kimura, Sci. Rep. **3**, 3031 (2013).
[34] H. Qin, J. Shi, Y. Cao, K. Wu, J. Zhang, E. W. Plummer, J. Wen, Z. J. Xu, G. D. Gu, and J. Guo, Phys. Rev. Lett. **105**, 256402 (2010).
[35] X. Zhu, Y. Cao, S. Zhang, X. Jia, Q. Guo, F. Yang, L. Zhu, J. Zhang, E. W. Plummer, and J. Guo, Rev. Sci. Instrum. **86**, 083902 (2015).
[36] H. Ibach, F. C. Bocquet, J. Sforzini, S. Soubatch, and F. S. Tautz, Rev. Sci. Instrum. **88**, 033903 (2017).